Examination of Flow and Heat Transfer Phenomena in Ducts with Dimples and Protrusions

O.M. Oyewola[1,2], M.O. Petinrin[2], M.A. Gbolasere[2], T.T. Olugasa[2]
[1]School of Mechanical Engineering, Fiji National University, Suva, Fiji
[2]Department of Mechanical Engineering, University of Ibadan, Ibadan, Nigeria
[1]oooyewola001@gmail.com, [2]olanrewaju.oyewola@fnu.ac.fj

***Abstract*-- Dimples and protrusions create effective flow structure by improving fluid-surface interactions and fluid-mixing in ducts for thermal enhancement with minimal pressure losses. The experimental investigation of the effects of dimples and protrusions in the form of smooth surface duct, teardrop dimpled and teardrop protruded duct on flow and heat transfer characteristics were examined. Measurements of temperature, pressure drop and velocity were carried out in an experimental test rig and data collected were used to evaluate the heat transfer, flow friction, and the overall thermal performance of the three test ducts for the Reynolds number ranges from 30,000 to 57,000. The results show that with reference to the smooth duct, the Nusselt number of dimpled duct increases by 134.4% while those of protruded duct increases by 41.6%. Further, the heat transfer augmentation ranges from 1.53 to 4.76 and 1.07 to 2.32 for dimpled duct and protruded duct, respectively. In addition, the protruded duct demonstrated a higher friction factor in the range of 1.48 to 2.25 times that of the smooth duct, while dimpled duct friction factor increases in the range of 1.10 to 1.31. The overall result suggests that the dimpled duct have the best thermal-hydraulic performance as revealed by the performance evaluation criteria.**

***Index Term*-- Protrusions, dimples, thermal performance, friction factor, normalized Nusselt number**

1. INTRODUCTION

Improving the performance of fluid and thermal equipment at lower energy cost has been the focus of engineers, using various surface structures which are not limited to extended surfaces, treated surfaces and rough surfaces (Turnow et al., 2012, 2003; Umavathi and Shekar, 2014; Xie et al., 2011). Extended surfaces or fins are added to heat transfer surfaces to augment the quantity of heat required to be removed from such surfaces with the available temperature difference and convective heat transfer coefficient (Boumaza and Omara, 2015; Burgess and Ligrani, 2005). This is a common practice when a surface is in interaction with gaseous fluid of low convective heat transfer coefficient, and this involves various configurations, shapes and sizes of the extended surfaces (Umavathi and Shekar, 2014).

The knowledge of the best configuration and shapes that will facilitate heat transfer best will take cooling of channels and engines to another level. Ruck et al.(2018) reported that surface with V-shaped ribs gave better heat transfer enhancement than surface with transverse ribs. Taslim et al.(2016) also found that heat transfer performance of the orthogonal ribbed channel was less than that of V-ribbed channel. Park et al.(1992) presented in their study on effect of channel aspect ratios, AR (width-height ratio) with ribs set at different angles of attack (30°, 45°, 60° and 90°) that the channels with AR < 1 showed better heat transfer performance than those with AR > 1 while 45°/60° ribbed angled channel gave the best for AR < 1, 30°/45° ribbed had better performance in AR > 1 category, and 60°/45° for squared ribbed channel.

Studies have shown that dimples and protrusions enhance rate of turbulence intensities in close ducts thereby augmenting the heat transfer rates from the surfaces with comparatively minimum pressure loss as compared with other types of heat transfer augmentation devices such as pins, fins, and rib turbulators (Xie et al., 2018). It has also been reported that protrusions enhance flow mixing and shedding in channels(Jang et al., 2018). As the choice of any of the augmentation devices, their pattern and placements does not only cause the braking of thermal boundary layers but also induce agitation in the boundary layer (Mahmood and Ligrani, 2002; Shen et al., 2016). In the numerical analysis conducted by Bi et al.(2013) on convective cooling in mini-channels with cylindrical grooves, low fins and dimples using the field synergy principle for Reynolds number ranged 2700 – 6100, the dimpled mini-channel was reported to have the highest performance based on the relative thermal and flow characteristics.

It is important to know that size, shape, configuration and arrangement of dimples on shape affects the rate of heat transfer enhancement. Most researchers have carried out experiments with different configurations, novel non-spherical dimple shapes and compare them to deduce which enhances heat transfer better. Yemin et al.(2017) experimentally investigated effect of protrusion spacings on the heat transfer rate in a test channel, considering protrusion pitch to print diameter ratios: S/D= 1.125, 1.25, 1.5 and 2. It was observed that S/D= 1.125 had the highest average Nusselt number and this performance decreases with increase in pitch ratio. Burgess and Ligrani

(2005) performed an experimental study on the influence of depth of dimples at fixed print diameter in a cooling channel, it was shown that for the range of Reynolds number (9,940 to 74,800) the local and average Nusselt number increase with the depth of the dimples. However, Xie et al. (2018) had shown that heat transfer rate and form friction increase, and overall thermal and hydraulic performance decreases with height of protrusion. Further, Rao et al.(2015) carried out both experimental and numerical study on different shapes (spherical, teardrop, elliptical, and inclined elliptical) of dimples of the same depth in channels at varying Reynolds number ranging from 8,500 – 60,000. Their study showed that the dimple structures significantly affect heat and flow structure of the channels. It was reported that the teardrop dimpled channel and elliptical dimpled channel showed the highest and lowest heat transfer, respectively as compared with spherical dimpled channel, while elliptical dimpled channel had comparatively the same heat and flow characteristic with the spherical dimpled channel.

Thus, studies have shown that surfaces with dimples/protrusions showed a better thermal performance in comparison to other geometries such as the spherical, elliptical, and inclined elliptical. However, previous studies have only considered dimples or protrusions on only one side of the channels or ducts or two opposite plates in fully developed flow regime, studies of these surfaces on all the four sides are sparse in literature for both developing and fully developed flow. Thus, there is continuous need for developing novel geometries and shapes of impressions and protrusions to achieve a higher overall heat transfer performance for industrial application. Therefore, this experimental work is focused on the thermo-hydraulic characteristics of flow in developing flow regime inside ducts with embossed teardrop dimples and embossed teardrop protrusion on the four walls in relation to a smooth surface duct.

2. Experimental Setup and Data Reduction

2.1 Dimple and Protrusion Pattern on Test Sections

The arrangement of the dimple and protrusion pattern is the traditional arrangement of chequered grooves on the plate as obtained from store. Two rectangular (dimpled and protruded) ducts, each of 50 mm square cross-section and 0.5 m long, were fabricated from the grooved plates while another duct of the same size was produced from smooth plates. Figures 1-3 show the details of the geometry, arrangement and dimensions (in millimeter) of the dimples and protrusions in each of the ducts.

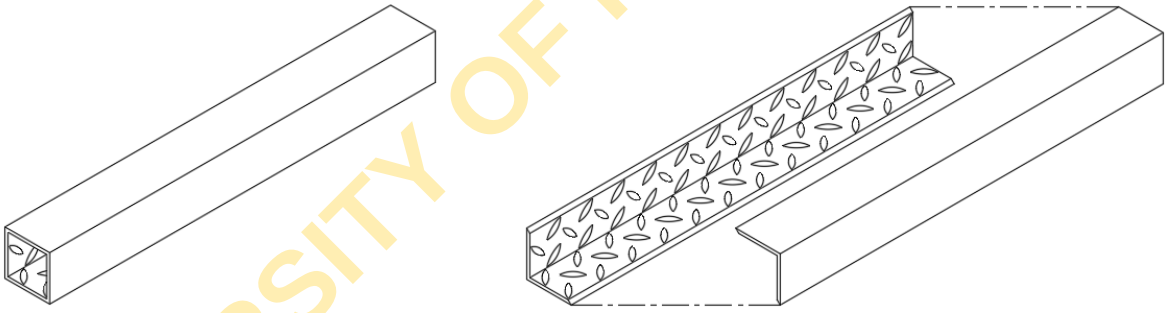

Fig. 1. The isometric and split views of either dimpled or protruded duct

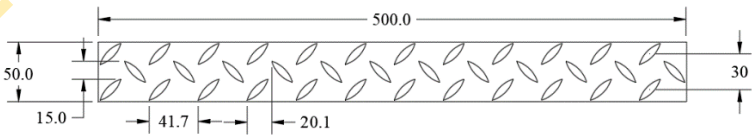

Fig. 2. Arrangement of for dimples/protrusions on each side of the duct (dimensions in mm)

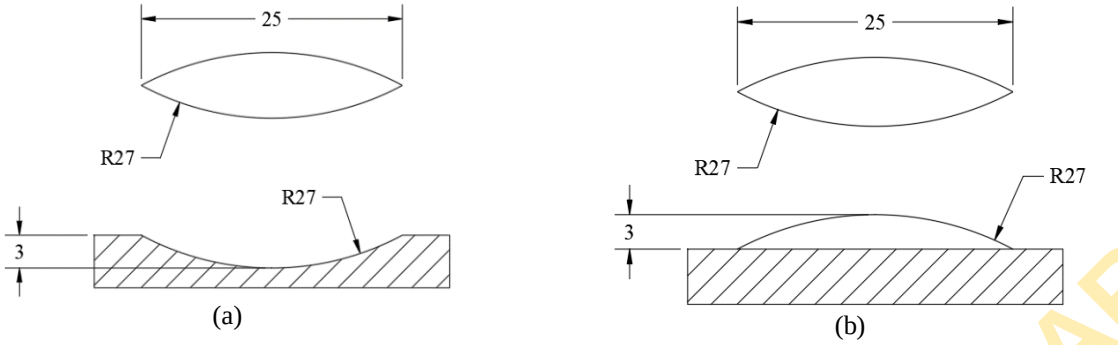

Fig. 3. Geometrical shapes of (a) dimple and (b) protrusion (dimensions in mm)

2.2 Experimental Setup

The complete setup comprises of a variable 10A blower, a variac, 1500W heating element, a digital temperature read out device, a pitot tube, and two digital manometers. The Experimental rig as seen in Figures 4 comprises of the test section of 50mm inside square section insulated by another 70mm square section, both sections 0.5m long. The insulating material used is fiberglass compacted into the pocket created by overlapping the two sections. The test section has six 15 mm diameter ports of equal spaces. The first and the last were used as differential pressure ports, while the middle four were used to accommodate thermocouples for measuring the temperature over the length of the channel. The inlet structure consists of a flow straightener and a reducer. The flow straightener was a honey-comb structure of pieced straws together. The temperature read out device was connected to five probes of thermocouples (±0.18% uncertainty) to measure four temperature points in the test section and the exit temperature. In this present work, in order to maintain developing flow regime within each of the duct, the length of the test section was shortened to accommodate ducts, and the duct length was also cut to no more than ten times its hydraulic diameter (Bergman et al., 2011).

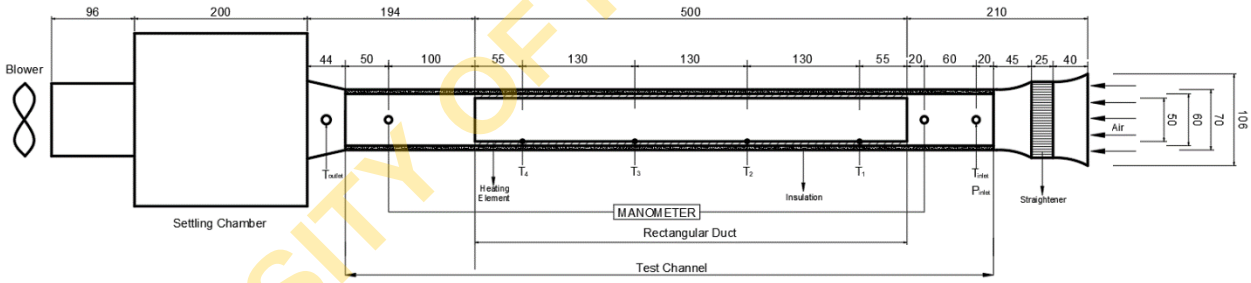

Fig. 4. The schematic arrangement of the experimental rig (dimensions in mm)

2.3 Experimental Procedure

To provide uniform heating the test channel (dimpled, protruded, or smooth) is being wound by a 1500W spring-type electric heating element and inserted into the fiberglass insulated test-section. The heating element was regulated to ensure constant temperature at the wall surfaces. Four Type-K thermocouples were installed in the four ports of the test chamber to measure the wall temperatures. As seen in Figure 5, two tubes were installed at the inlet and outlet of the test section and connected to a digital manometer which gives the value of the differential pressure. Another digital manometer was used in measuring the dynamic pressure of air from the blower for various speeds activated by the variac. The test section was enclosed by a pocket tightly packed with fiberglass in order to reduce heat lost from test section to surroundings.

Fig. 5. Experimental Setup showing points of measurements on the experimental rig

The thermocouple probes were fixed at an estimated depth of 100mm downstream of the outflow of the flow channel. The values measured from these probes are used in calculating the mean temperature of the flow leaving the test channel. Wall temperatures, pressure drop and the pressure of the blower were also taken as the speed of the blower was being varied. The test section was enclosed by a pocket tightly packed with fiberglass in order to reduce heat lost from test section to surroundings.

3. Data Reduction

The obtained data was analysed to determine the thermal-hydraulic characteristics of the three channels. The heat added to the fluid pass through the ducts is determined from

$$Q = \dot{m} c_p \left(T_{out} - T_{in} \right) \tag{1}$$

The average heat transfer coefficient on each of the walls of the ducts is calculated from

$$h = \frac{Q}{A_s \Delta T_{LM}} \tag{2}$$

The averaged Nusselt number from the heat transfer duct surfaces is defined by

$$Nu = \frac{h d_h}{k} \tag{3}$$

where d_h is the channel hydraulic diameter of the duct and $k$is the fluid thermal conductivity.
Thus, the log mean temperature difference, ΔT_{lm} between the heating wall and the cool air flow is determined from (Bergman et al., 2011; Rao et al., 2015)

$$\Delta T_{lm} = \frac{\left(T_w - T_{in}\right) - \left(T_w - T_{out}\right)}{In\left(\frac{T_w - T_{in}}{T_w - T_{out}}\right)} \tag{4}$$

where T_w is the average temperature of the fluid-state surface of the test section.
The friction factor is obtained from the pressure drop across the duct as

$$f = \frac{\Delta P}{\left[\left(\frac{L}{D_h}\right)\left(\frac{1}{2}\rho V^2\right)\right]} \tag{5}$$

The duct inlet velocity was deduced from the dynamic pressure obtained as a result of the difference between the stagnation pressure, p_{stag} and static pressure, p_s readings from the duct inlet as (Cengel and Cimbala, 2006)

$$V = \sqrt{\frac{2\left(p_{stag} - p_s\right)}{\rho}} \tag{6}$$

while the Reynolds number was calculated from

$$\mathrm{Re} = \frac{\rho V d_h}{\mu} \tag{7}$$

The heat transfer characteristics and friction factor for fully developed flow in a smooth duct serve as the base data for comparing the performance of the test surfaces, thus in effect help to evaluate efficiently the thermal performance of the dimpled channels, which can be represented by a universal evaluation parameter of a heat transfer unit known as the Performance Evaluation Criteria (PEC) (Bi et al., 2013; Xie et al., 2018)

$$PEC = \frac{Nu/Nu_0}{\left(f/f_0\right)^{1/3}} \tag{8}$$

where Nu/Nu_0 is the normalized Nusselt number, that is, the ratio of the Nusselt number of the dimpled/protruded channel to that of the smooth channel while f/f_0 is the friction factor ratio of dimpled/protruded channel to smooth channel.

The Uncertainties

The standard uncertainty analysis used to determine the uncertainties from the experiments were adopted from Moffat (1988) amd Olivier (2009). For a desired variable, $R = f(x_i)$, the uncertainty is estimated from uncertainties, δx_i from a number of independent variables as

$$\delta R = \left[\sum_{i=1}^{n} \left(\frac{\partial R}{\partial x_i} \delta x_i \right)^2 \right]^{1/2} \quad (9)$$

while the uncertainty of a single measured value from bias error, *B*and precision error, *P* of measurement is calculated from

$$\delta x_i = \sqrt{B_i^2 + P_i^2} \quad (10)$$

Using the measuring instruments, the maximum uncertainty for the air speed was ±0.5%, flow rate was ±2.45%, the pressure drop was estimated to be ±2.06% and. The temperature uncertainties equaled ±0.2°C, the net heating power *Q* calculated was ±4.68%. The measurement uncertainties determined for Reynolds number, friction factor and Nusselt number were about ±3%, ±4.8% and ±7.6%, respectively.

4. Results and Discussion

Flow through the three different rectangular ducts in test section was investigated with seven different and increasing velocities, spanning the range of Reynolds number from 30,000 to 57,000. Interestingly, it signifies flow in moderate to high Reynolds numbers which have a lot of industrial applications. The average Nusselt numbers of the three ducts in variation with Reynolds number are as shown in Figure 6. It can be seen that the Nusselt number increases with increase in Reynolds number. The Embossed-teardrop dimpled duct shows the highest values of Nusselt number, having values ranging from 242 to 778 with about 134.4% increase over that of the smooth duct. The duct with protrusion also demonstrated an increase of about 41.6% over smooth duct. Figure 7 presents the average Nusselt number ratio for the three test channels, this is the ratio of flow Nusselt number from the ducts as compared with that of the smooth duct. It can be seen that the normalized Nusselt number of both the dimpled and protruded surfaces seem to be less dependent on the Reynolds number when it is greater than 38,000. The normalized heat transfer Nu/Nu_0 of the dimpled and protruded ducts typifies the heat transfer enhancement of dimpled and protruded ducts over the smooth duct. The heat transfer augmentation from the smooth duct to an embossed teardrop dimple ranges from 1.53 to 4.76 while to embossed teardrop protruded duct ranges from 1.07 to 2.32. It worth mentioning that there is a poor agreement between the result for smooth duct/channel and Dittus-Boelter correlation. This is not surprising since Dittus-Boelter correlation was formulated for fully developed flow.

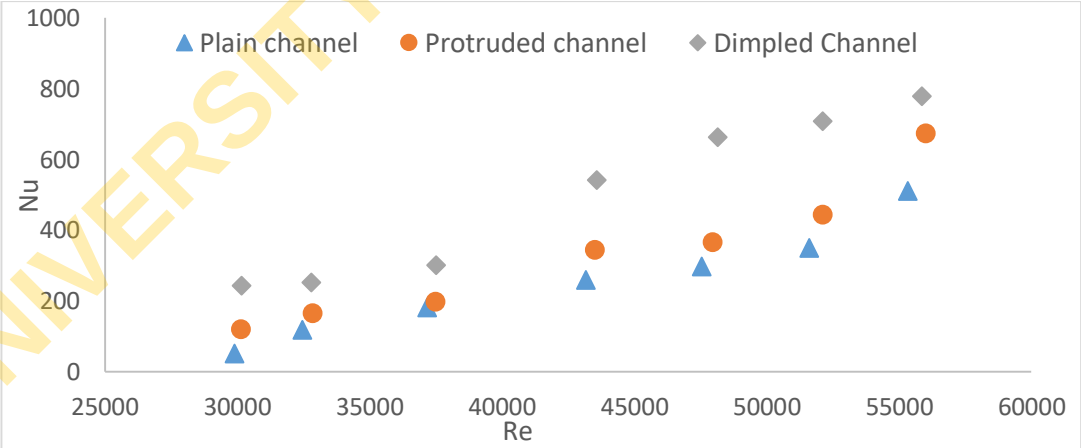

Fig. 6. The variation of averaged Nusselt number with Reynolds number in the various test channels

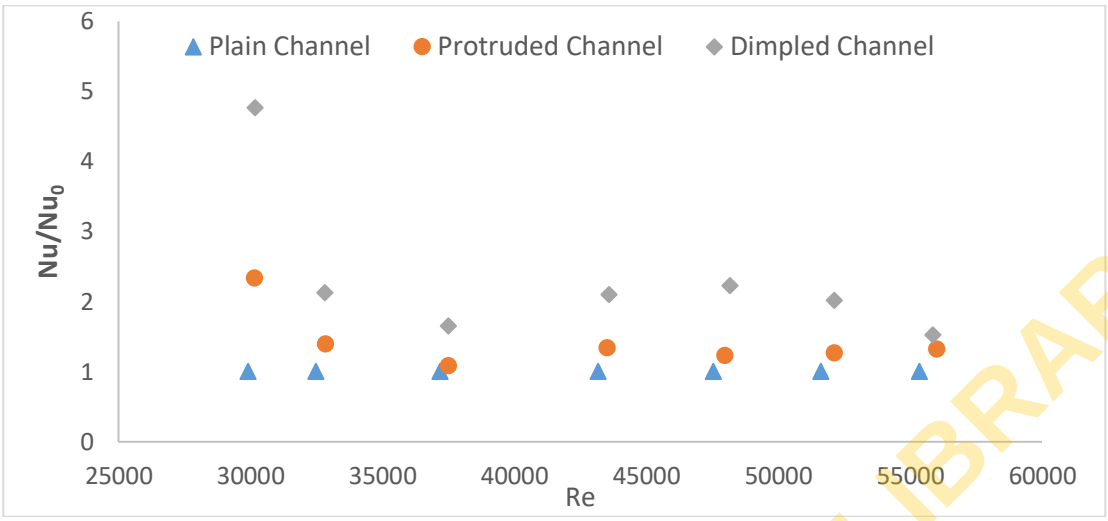

Fig. 7. The variation of Normalized average Nusselt number with Reynolds number in the various test channels.

The flow friction behaviors in the test ducts for the Reynolds number range are as depicted in Figure 8. From all the experimental observations through the ducts, it can obviously be seen that the friction factors averagely decrease with Reynolds number. The dimpled and protruded ducts have about 21.2 and 95.5% increase in friction factor as compared with smooth duct, respectively. Figure 9 shows variation of the friction factor ratio with Reynolds number for the three ducts as against that of the smooth duct. The flow friction factor in the dimpled duct is about 1.10-1.31 times that of the smooth duct while that of protruded duct is higher, and it is about 1.48-2.25 times that of the smooth duct. Overall, the protruded suffers the most pressure loss, while the smooth surface displays a fairly better hydraulic performance than the embossed-teardrop dimpled channel. This could be as a result of the obstruction to flow by the protrusion heights which enables more fluid interaction with the walls of the channel thereby increasing the friction generated between the walls of the channel and the fluid flow.

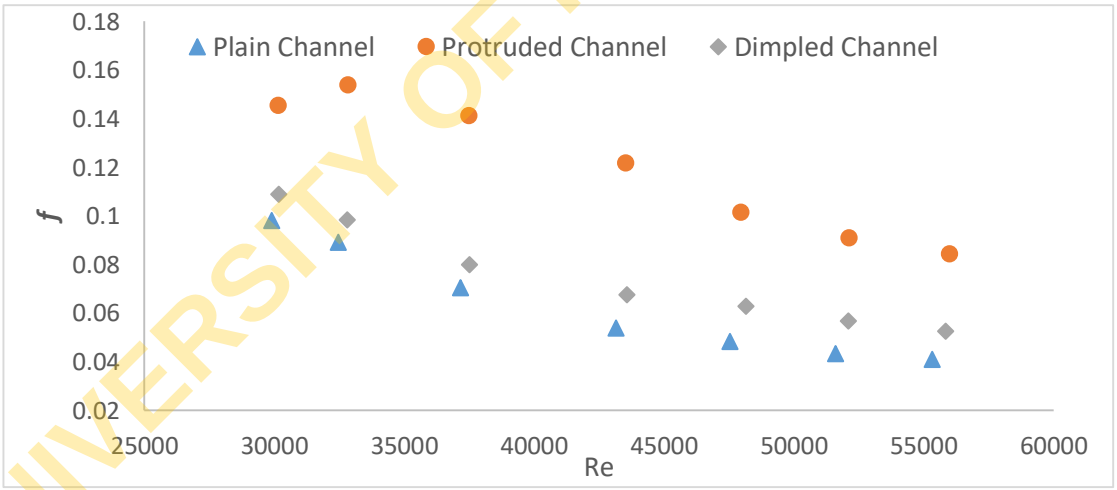

Fig. 8. The variation of Friction factors with Reynolds number in the various test channels

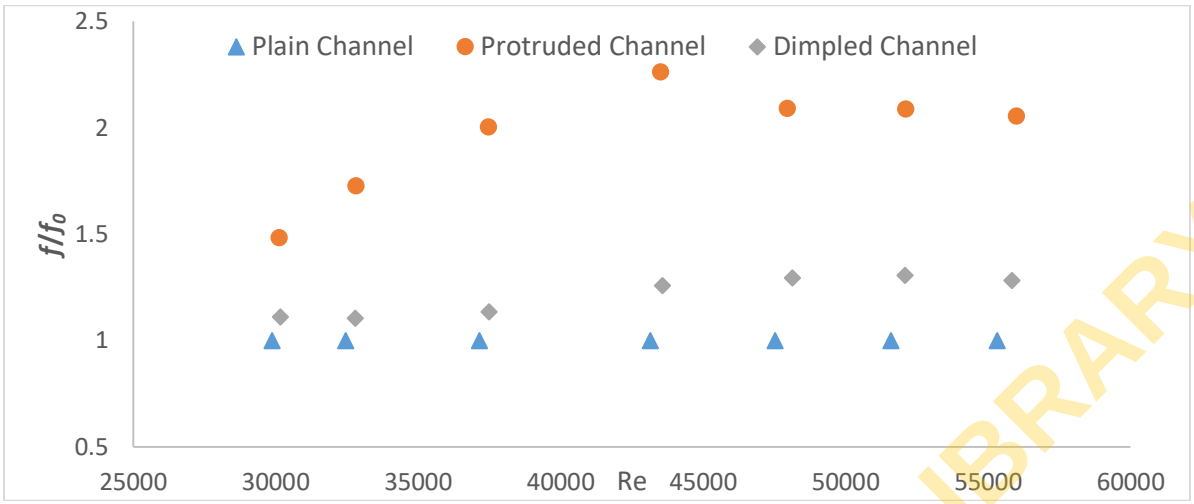

Fig. 9. The variation of Friction factor ratios with Reynolds number of the various test ducts

Figure 10 presents the overall thermal-hydraulic performance of the three-test channel, which is obtained as the ratio of the normalized average Nusselt number of the ducts at varying Reynolds number against their corresponding flow friction factors. It can be seen that the dimpled duct have higher values of thermal-hydraulic performance compared to the other two ducts which is relatively not influence by change in Reynolds number. Figure 11 shows the ratio of normalized Nusselt number to wetted surface area of the ducts. From this figure, the dimpled and protruded ducts have 104 and 23% increase over that of the smooth duct. Although, the wetted surface areas of the dimpled and protrusion ducts are the same but their contribution to thermal performance are not the same. The result suggests that dimpled duct have better overall thermal performance and the sensitivity to change in Reynolds number is not significant.

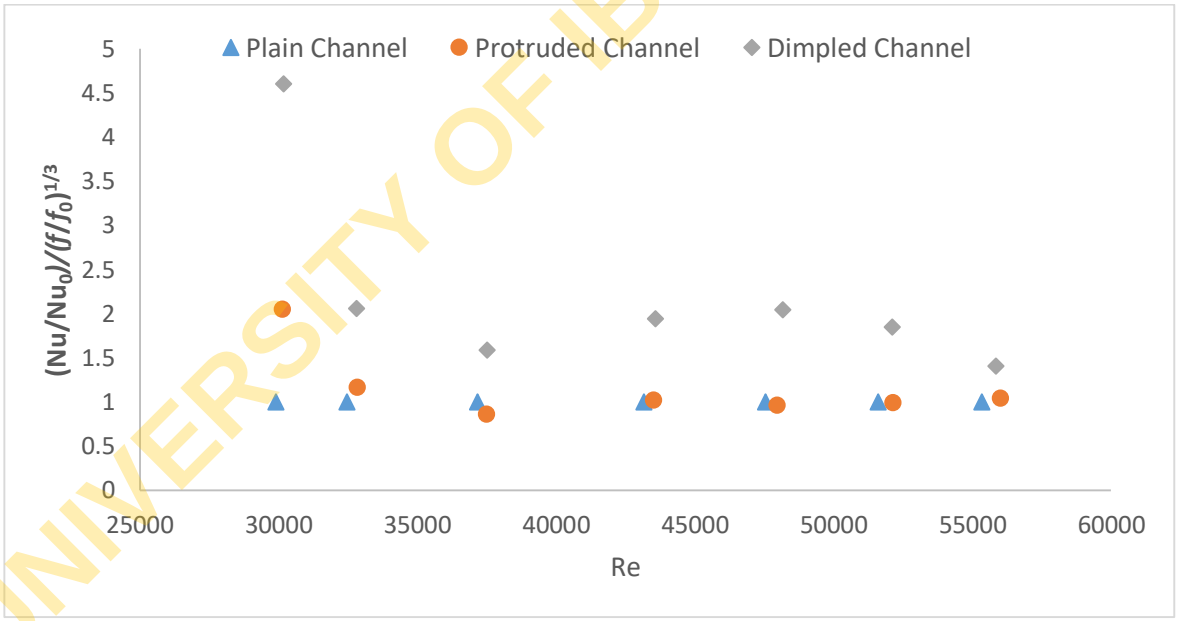

Fig. 10. The thermal-hydraulic performance of the three ducts over the range of Reynolds numbers

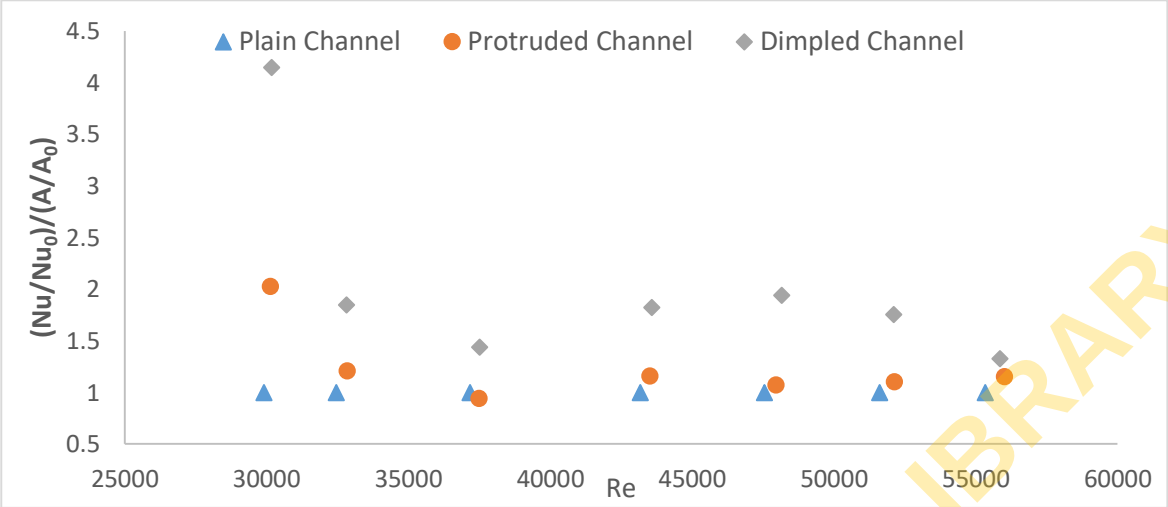

Fig. 11. The thermal performance of the three ducts over the range of Reynolds numbers

5. Conclusion

Experimental study was comparatively carried out in smooth, dimpled, and protruded ducts in order to examine their effects on the flow and heat transfer phenomena. The friction factor, heat transfer enhancement and the overall heat transfer performance were determined for each of the test ducts from the measurements of velocity, pressure drop and temperature over the Reynolds number range of 30,000 to 57,000. It was inferred from the study that heat transfer rate in a duct was increased with increase in Reynolds number. The dimpled duct has a higher Nusselt number follow by protruded duct than the smooth duct and it accounted for 134.4 and 41.6%, respectively. However, Protruded duct gave the highest friction factor with approximately 95.5% more than the smooth duct. Moreover, the heat transfer augmentation ranged from 1.53 to 4.76 and 1.07 to 2.32 for dimpled duct and protruded duct, respectively. Thus, the results showed that the dimpled duct was most effective in terms of heat transfer augmentation and by extension have a considerable friction factor, minimal pressure loss and better overall thermal performance.

Acknowledgement

Nil

Competing Interests

Not applicable

Nomenclature

Abbreviations and Symbols

A_s	Surface area of the duct (m^2)
c_p	Specific heat capacity at constant pressure (J/kgK)
d_h	Hydraulic diameter (m)
f	Friction factor
k	Thermal conductivity (W/mK)
L	Duct length (m)
Re	Reynolds number
Δp	Pressure drop (Pa)
h	Heat transfer coefficient (W/m^2K)
$\dot{m}$	Mass flow rate (kg/s)
Nu	Nusselt number
PEC	Performance evaluation criteria
Q	Heat transfer rate (W)
T	Temperature (K)
V	Flow velocity (m/s)
w	Plate width (m)
ΔT_{lm}	Log mean temperature difference

Greek Symbols

ρ	Density of fluid (kg/m^3)
μ	Dynamic viscosity of fluid (Pas)

Subscripts

in	Inlet
out	Outlet
s	Static
stag	Stagnation
w	Wall

References

[1] Bi, C., Tang, G. H., Tao, W. Q., 2013. Heat transfer enhancement in mini-channel heat sinks with dimples and cylindrical grooves. Appl. Thermal Eng. *55*, 121–132. https://doi.org/10.1016/j.applthermaleng.2013.03.007

[2] Burgess, N. K., Ligrani, P. M., 2005. Effects Of Dimple Depth on Channel Nusselt Numbers and Friction Factors. J. Heat Trans. 127, 839–847.

[3] Jang, H. N., Park, J. S., Kwak, J. S., 2018. Experimental study on heat transfer characteristics in a ribbed channel with

dimples, semi-spherical protrusions, or oval protrusions. Appl. Thermal Eng. 131, 734–742. https://doi.org/10.1016/j.applthermaleng.2017.12.030
[4] Mahmood, G. I., Ligrani, P. M., 2002. Heat transfer in a dimpled channel: combined influences of aspect ratio, temperature ratio, Reynolds number, and flow structure. Int. J. Heat Mass Trans. 45, 2011–2020.
[5] Moffat, R. J., 1988. Describing the Uncertainties in Experimental Results. Exp. Thermal Fluid Sci. 1, 3–17.
[6] Olivier, J. A., 2009. Single-Phase Heat Transfer and Pressure Drop of Water Cooled at a Constant Wall Temperature inside Horizontal Circular Smooth and Enhanced Tubes with Different Inlet Configurations in the Transitional Flow Regime. Ph.D. Thesis, Department of Mechanical and Aeronautical Engineering, University of Pretoria, Pretoria.
[7] Park, J. S., Han, J. C., Huang, Y., Ou, S., Boyle, R. J., 1992. Heat transfer performance comparisons of five different rectangular channels with parallel angled ribs. Int. J. Heat Mass Trans. 35 (11), 2891–2903.
[8] Rao, Y., Feng, Y., Li, B., Weigand, B., 2015. Experimental and Numerical Study of Heat Transfer and Flow Friction in Channels With Dimples of Different Shapes. J. Heat Trans. 137 (031901), 1–10. https://doi.org/10.1115/1.4029036
[9] Ruck, S., Köhler, S., Schlindwein, G., Arbeiter, F., 2018. Heat transfer and pressure drop measurements in channels roughened by variously shaped ribs on one wall. Exp. Heat Trans. 31 (4), 334–354. https://doi.org/10.1080/08916152.2017.1410506
[10] Shen, Z., Xie, Y., Zhang, D., 2016. Experimental and numerical study on heat transfer in trailing edge cooling passages with dimples/protrusions under the effect of side wall slot ejection. Int. J. Heat Mass Trans. 92, 1218–1235.
[11] Taslim, M. E., Li, T., Kercher, D. M., 2016. Experimental Heat Transfer and Friction in Channels Roughened with Angled, V-Shaped, and Discrete Ribs on Two Opposite Walls. Trans. ASME. 118 (January 1996), 20–28.
[12] Turnow, J., Kornev, N., Zhdanov, V., Hassel, E., 2012. Flow structures and heat transfer on dimples in a staggered arrangement. *Int. J. Heat Fluid Flow*. 35, 168–175. https://doi.org/10.1016/j.ijheatfluidflow.2012.01.002
[13] Turnow, J., Zhdanov, V., Hassel, E., Kornev, N., 2011. Flow structures and heat transfer on dimpled surfaces, Proc. TSFP. 1–6.
[14] Xie, G., Sundén, B., Zhang, W., 2011. Comparisons of Pins/Dimples/Protrusions Cooling Concepts for a Turbine Blade Tip-Wall at High Reynolds Numbers. J. Heat Trans. 133 (061902), 1–9. https://doi.org/10.1115/1.4003558
[15] Xie, S., Liang, Z., Zhang, L., Wang, Y., Ding, H., Zhang, J., 2018. Numerical investigation on heat transfer performance and flow characteristics in enhanced tube with dimples and protrusions. Int. J. Heat Mass Trans. 122, 602–613. https://doi.org/10.1016/j.ijheatmasstransfer.2018.01.106
[16] Yemin, O., Wae-Hayee, M., Nuntadusit, C., 2017. Experimental study on the heat transfer enhancement of the effect of teardrop protrusion-to-protrusion spacing Experimental study on the heat transfer enhancement of the effect of teardrop protrusion - to - protrusion spacing. In IOP Conference Series: Materials Science and Engineering (pp. 0–9). IOP Publishing. https://doi.org/10.1088/1757-899X/297/1/012065